3752 *Chem. Mater.* **2010,** *22,* 3752–3761
DOI:10.1021/cm100750z

CHEMISTRY OF MATERIALS
Article

Synthesis of n-type $CuInS_2$ Particles Using *N*-methylimidazole, Characterization and Growth Mechanism

Fabrice M. Courtel,*[,†,‡] Amer Hammami,[§] Régis Imbeault,[§] Grégory Hersant,[⊥] Royston W. Paynter,[†] Benoît Marsan,[§] and Mario Morin[§]

[†]*Centre Énergie, Matériaux et Télécommunications - Institut National de la Recherche Scientifique (INRS), 1650 boulevard Lionel-Boulet, Varennes, Québec J3X 1S2, Canada,* [§]*Département de Chimie, Université du Québec à Montréal (UQÀM), C.P. 8888, Succursale Centre-ville, Montréal, Québec H3C 3P8, Canada, and* [⊥]*Department of Chemistry, Concordia University, 7141 Sherbrooke Street West, Montréal, Québec H4B 1R6, Canada.* [‡]*Current address: National Research Council Canada, 1200 Montreal Road, Ottawa, Ontario K1A 0R6, Canada*

Received March 14, 2010. Revised Manuscript Received May 1, 2010

We report on the growth of $CuInS_2$ n-type semiconductive particles, prepared using *N*-methylimidazole, as a solvent and/or a complexing agent, as well as their chemical and electrochemical properties. XPS, EDX and ICP-AES have shown that an excess of indium was obtained, which was greater at the surface ($CuIn_{1.19}S_{1.7}$ at 500 °C) than in the bulk ($CuIn_{1.07}S_{1.9}$ at 500 °C). Solid state Raman spectroscopy revealed two crystalline phases: chalcopyrite and the so-called copper−gold phase, and by increasing the annealing temperature of the particles, the formation of the chalcopyrite phase is favored. UV−visible measurements showed that the n-type $CuInS_2$ possesses a direct bandgap energy of 1.55 eV. To perform the capacitance measurements on a $CuInS_2$ film by EIS, we used two organic redox couples in nonaqueous media: 5-mercapto-1-methyltetrazolate (T^-)/di-5-(1-methyltetrazole) disulfide (T_2), and 5-trifluoromethyl-2-mercapto-1,3,4-thiadiazolate (G^-)/5,5′-bis(2-trifluoromethyl-1,3,4-thiadiazole) disulfide (G_2). Using these redox couples, we determined Fermi levels of −4.51 eV and −4.53 eV, and majority charge carrier densities of 2.8×10^{18} and 9.6×10^{18} cm^{-3}, respectively. According to the energy level diagram of the $CuInS_2$/electrolyte interface, the G^-/G_2 redox couple is expected to lead to a more efficient device. The present work shows that the complexation of the metal ions and the negative charge on sulfur anions play a key role in the mechanism of formation of $CuInS_2$ particles. In situ Raman spectroscopy measurements showed that an indium−sulfur precursor is formed prior to the formation of $CuInS_2$ particles. Indeed, if an indium−sulfur precursor is formed prior to the reaction of sulfur with copper, a much better control of the n-type $CuInS_2$ properties is obtained. This explains the excess of indium at the surface of the $CuInS_2$ particles, as well as its n-type semiconductivity.

Introduction

Commercially available solar cells are based on a solid−solid junction between two semiconductors. n and p doped silicon are widely used in this kind of cells but they require an high silicon grade. Chalcopyrite semiconductors, such as $CuInS_2$ and $CuInSe_2$, are also good candidates for photovoltaic applications because of their favorable optical properties. For instance, $CuInS_2$ has a high absorption coefficient of 1×10^5 cm^{-1} (at 730−750 nm) that is 10 times greater than that of CdTe.[1] This ensures a complete absorption of photons in micrometric range coatings. $CuInS_2$ exhibits a direct bandgap energy of 1.5 eV that matches closely the solar spectrum.[2] Moreover, in 1975, Meese et al. determined that $CuInS_2$ has a high theoretical conversion efficiency of 30%.[3] However, the control of stoichiometry is a major difficulty in the synthesis of ternary materials. Most of the $CuInS_2$ synthetic methods reported in the literature yield material with p-type semiconductivity. However, some colloidal methods yield n-type $CuInS_2$[4−6] that are In-rich[7] and might be used in photovoltaic and photoelectrochemical cells.

We recently reported on the growth mechanism of n-type $CuInS_2$ particles prepared using a modified Czekelius's colloidal method, as well as their chemical and

*Corresponding author. Phone: (613) 993-8573. Fax: (613) 949-4184. E-mail: Fabrice.Courtel@nrc-cnrc.gc.ca.

(1) Mitchell, K.; Fahrenbruch, A. L.; Bube, R. H. *J. Appl. Phys.* **1977**, *48*(2), 829–830.
(2) Moller, H. J., *Semiconductors for Solar Cells*. Artech House: Boston, 1993.
(3) Meese, J. M.; Manthuruthil, J. C.; Locker, D. R. *J. Am. Phys. Soc.* **1975**, *20*, 696–703.
(4) Czekelius, C.; Hilgendorff, M.; Spanhel, L.; Bedja, I.; Lerch, M.; Müller, G.; Bloeck, U.; Su, D.-S.; Giersig, M. *Adv. Mater.* **1999**, *11* (8), 643–646.
(5) Castro, S. L.; Bailey, S. G.; Raffaelle, R. P.; Banger, K. K.; Hepp, A. F. *J. Phys. Chem. B* **2004**, *108*(33), 12429–12435.
(6) Arici, E.; Hoppe, H.; Reuning, A.; Sariciftci,N. S.; Meissner, D. In *CIS Plastic Solar Cells, Proceedings of the 17th European Photovoltaic Solar Energy Conference*; Munich, Germany, October 22−26, 2001; James and James: London, 2001;pp 61−63.
(7) Yoshino, K.; Nomoto, K.; Kinoshita, A.; Ikari, T.; Akaki, Y.; Yoshitake, T. *J. Mater. Sci.: Mater. Electron.* **2008**, *19*(4), 301–304.

Published on Web 05/17/2010

electrochemical properties.[8] This method uses triphenyl phosphite (TPP) as a ligand, which complexes Cu^+ and In^{3+} species, and hexamethyldisilathiane as an organic sulfur source. An excess of indium was obtained in the material, which was greater at the surface than in the bulk with an In/Cu atomic ratio of 1.45 and 1.04, respectively. The n-type semiconductivity was confirmed from capacitance measurements. The excess of indium at the surface of the particles was explained from in situ Raman spectroscopy measurements that demonstrated the faster reactivity of hexamethyldisilathiane with copper as compared with indium. Slowing down the reactivity of copper with the sulfur source is the major challenge in order to be able to control the indium excess in the bulk and at the surface.

In this work, we report a synthetic method for $CuInS_2$ that uses *N*-methylimidazole (NMI) as an anhydrous solvent and/or a complexing agent; no ligand such as TPP is needed. Furthermore, contrarily to our previous work,[8] an inorganic sulfur source is used. This new method was developed to reduce the level of organic contamination. To the best of our knowledge, it is the first time that such a synthetic method is reported.[9] NMI is well-known to dissolve numerous metal salts. It is a transparent liquid with a melting point of −60 °C and a boiling point of 198 °C. It has also found use as an ionic liquid precursor; for instance, NMI can be alkylated in order to form dialkyl imidazolium salts. Depending on the alkylating agent and the counteranion, various ionic liquids are obtained.[10,11] Here, indium and copper salts are dissolved separately in NMI and a Li_2S suspension in NMI is prepared. These solutions are used as reagents for the synthesis. Quantitative chemical analyses of the bulk and surface of the $CuInS_2$ particles are also reported. UV−visible absorption measurements and electrochemical characterization are performed on films made of $CuInS_2$ particles to determine the semiconductor bandgap energy and the electrical properties (type of semiconductivity, flatband potential, and majority charge carrier density). The growth of the $CuInS_2$ particles was followed by in situ Raman spectroscopy, which allowed us to propose a growth mechanism.

Experimental Methods

Materials. Except for tetra-*n*-butylammonium perchlorate, all chemicals were used as received. $InCl_3$ (anhydrous, 99.999%), CuI (99.999%), CuCl (99.999%), NMI (*N*-methylimidazole, 99+%, purified by redistillation), CH_3CN (anhydrous, 99.8%), 1-methyl-2-pyrrolidinone (NMP, 99+%, HPLC grade), polyvinylidene fluoride (PVDF, $M_w \approx 534\,000$ g mol^{-1}), $AgNO_3$ (>99%), $AgSO_3CF_3$ (99%), ferrocene (98%), ethylene carbonate (EC, 98%), and dimethyl carbonate (DMC, ReagentPlus, 99%) are from Aldrich. Tetra-*n*-butylammonium perchlorate (TBAP, 99+%, recrystallized in ethyl acetate) and Li_2S (99.999%) are from Alfa Aesar. Ethanol (100%, HPLC grade) and hexane (HPLC grade) are supplied by A&C and EMD, respectively. Argon (99.6%) is purchased from Praxair. The first redox couple used for the electrochemical characterization of the semiconductor is T^-/T_2, where T^- stands for 5-mercapto-1-methyltetrazolate ion produced in solution from 5-mercapto-1-methyltetrazole (HT, $C_2H_4N_4S$, 98%) commercially available from Aldrich, whereas the oxidized species di-5-(1-methyltetrazole) disulfide (T_2) was synthesized using a procedure described elsewhere.[12] The second redox couple is G^-/G_2, where G^- stands for 5-trifluoromethyl-2-mercapto-1,3,4-thiadiazolate ion produced in solution from the potassium salt KG and the oxidized species G_2 for 5,5′-bis(2-trifluoromethyl-1,3,4-thiadiazole) disulfide. KG and G_2 were synthesized using a procedure developed by Hersant et al.[13,14] The structures of the redox molecules are shown in the Supporting Information, S1.

Synthesis. *Method 1.* On the basis of a work previously reported,[8] Cu and In precursor solutions were prepared and mixed together with an inorganic sulfur source to form $CuInS_2$ particles. However, unlike our previous work,[8] no ligand such as TPP was used because the solvent (NMI) is able to dissolve halogenated metal salts. In an argon-filled glovebox, NMI solutions of $InCl_3$ (0.025 M) and CuI (0.060 M) were prepared. The solutions were kept under magnetic stirring for 30 min. As Li_2S is not soluble in NMI, three 20 min cycles of magnetic stirring were followed by ultrasonication to obtain a stable dispersion of 0.130 M of Li_2S in NMI (stable for ∼1 h). One equivalent of copper was mixed with 2 equiv. of indium and then two equivalents of sulfur were added at a rate of 2.5 mL min^{-1}. The Li_2S addition was done under magnetic stirring and immediately dark particles appeared. The magnetic stirring was then stopped, which was followed, 2 h later, by precipitation of the particles. The precipitate was filtered and rinsed with acetonitrile outside the glovebox in order to remove NMI and the lithium salts. The powder was then dried under a vacuum and annealed for 2 h at 350 °C under a vacuum (100 mTorr).

Method 2[9]. Compared to method 1, the addition order of the reagents has been changed. In an argon filled glovebox, solutions of $InCl_3$ (0.025 M, colorless) and CuCl (0.060 M, transparent green) were prepared in NMI and stirred for 30 min. The Li_2S suspension (0.130 M) was prepared as described in method 1. One and two-tenths equivalents of indium and 2.4 equiv. of sulfur were mixed in. Four 20 min cycles of magnetic stirring followed by ultrasonication were needed to obtain a transparent yellow solution. One equivalent of copper was then added at once. After 20 min, the mixture turned into an orange suspension. This suspension was heated for 3 h at 80 °C inside the glovebox and then cooled to room temperature. The resulting black suspension was filtered, rinsed with acetonitrile, and dried under a vacuum. The particles were then annealed for 2 h at different temperatures under a vacuum (100 mTorr).

Characterization. The crystalline phases of the $CuInS_2$ particles were obtained from X-ray diffraction (XRD, Siemens

(8) Courtel, F. M.; Paynter, R. W.; Marsan, B.; Morin, M. *Chem. Mater.* **2009**, *21*(16), 3752–3762.
(9) Hammami, A.; Marsan, B.; Courtel, F.; Morin, M. Processes for preparing chalcopyrite-type compounds and other inorganic compounds. Patent WO/2006/119621, PCT/CA2006/000738. 2006.
(10) Meindersma, W.; Maase, M.; De Haan, A. B. *Ullmann's Encyclopedia of Industrial Chemistry*; Wiley-VCH: Weinheim, Germany, 2007; Vol. Ionic liquids.
(11) Dupont, J.; Consorti, C. S.; Suarez, P. A. Z.; De Souza, R. F. *Org. Synth.* **2002**, *79*, 236–239.
(12) Philias, J. M.; Marsan, B. *Electrochim. Acta* **1999**, *44*(14), 2351–2363.
(13) Hersant, G. Préparation et caractérisations de nouveaux milieux électrolytiques quasi-transparents destinés à une application en pile solaire. Ph.D. Thesis, Concordia University−Université du Québec à Montréal, Montreal, Canada, in preparation.
(14) Hammami, A.; Marsan, B.; Armand, M.; Hersant, G. Redox Couples, Compositions and Uses Thereof. WO 2007/109907 and CA 2 541 232, (2007) 2006.

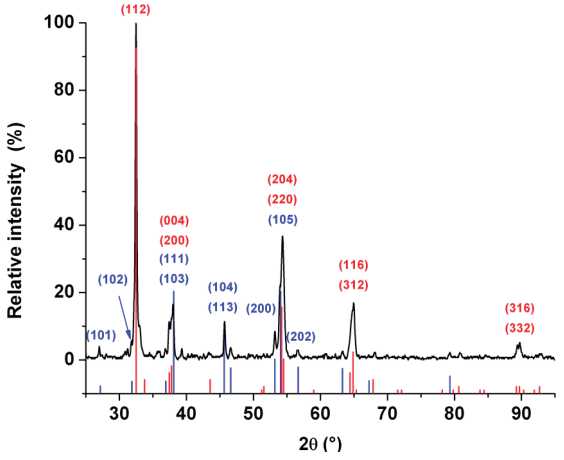

Figure 1. X-ray diffractogram of $CuInS_2$ particles obtained from experimental Method 1, annealed for 2 h at 350 °C under a vacuum (100 mTorr). In red lines, the $CuInS_2$ chalcopyrite (CH) structure (JCPDS-ICDD file 27-0159[15]) and in blue lines, the Cu_2S tetragonale chalcocite structure (JCPDS-ICDD file 72−1071).

D-5000, cobalt X-ray source, $K_{\alpha 1}$ λ, 1.7890 Å, step size 0.02°, 2s per step) and Raman spectroscopy (Renishaw RM 3000, λ_{ex}, 782 nm). The crystallite size was calculated using the XRD results and the Scherrer equation with a shape factor of 0.9,[15] and the particle size was estimated using scanning electron microscopy, SEM (Hitachi S-4300SE/N VP-SEM). The bulk stoichiometry was estimated by energy-dispersive X-ray analysis (EDX, EDAX detector integrated into the SEM) and inductively coupled plasma−atomic emission spectroscopy (ICP-AES, Jobin Yvon Horiba JY2000, λ_{Cu}: 223.008 nm and λ_{In}: 230.606 nm). The surface stoichiometry was determined by X-ray photoelectron spectroscopy (XPS, VG Escalab 220iXL, $\lambda_{Al\ achromatic}$: 1486.7 eV). Surface analysis of the particles, done by XPS, was also carried out in order to obtain the oxidation state of the elements and to detect surface contaminants. CuCl, CuI, $InCl_3$, and NMI UV−visible spectra were obtained in a sealed quartz cell under argon using a UV−visible spectrometer (Varian Cary 100 Bio). The bandgap energy of the $CuInS_2$ particles annealed at 500 °C for 2 h under a vacuum (100 mTorr), was determined from the UV−visible spectrum (Varian Cary 100 Bio) of a 10 μm thick film prepared on an ITO conducting glass substrate. To obtain the film, the ITO substrate was immersed in an acetronitrile suspension of $CuInS_2$ particles followed by evaporation of the solvent after withdrawal of the substrate.

Electrochemical impedance spectroscopy (EIS) was used to determine the type of semiconductivity, the Fermi level and the majority charge carrier density of a $CuInS_2$ film (multipotentiostat: solartron 1470 and frequency response analyzer: solartron 1255B). The EIS measurements were done in a one-compartment glass electrochemical cell with a three-electrode configuration as described elsewhere.[8]

Kinetics measurements, done by in situ Raman spectroscopy, were performed using solutions of 0.025 M $InCl_3$ in NMI, 0.060 M CuCl in NMI, the precursor yellow transparent solution and a 0.130 M suspension of Li_2S in NMI. All solutions were prepared and kept under argon during the entire experiment. All measurements were done with a Renishaw RM 3000 Raman spectrometer coupled with a Leica optical microscope. The chosen laser wavelength was 785 nm because it gave the best signal/noise ratio at a power density of 3 mW μm^{-2}. Because the solutions were prepared in normal glass vials, identification of the Raman vibrations of glass was done ($\bar{\nu}$: 430, 448, 670, 821, 877, 900, and 1035 cm^{-1}).

(15) Golub, B. D., *Elements of X-ray Diffraction*, 2nd ed.; Addison-Wesley: Amsterdam, 1978.

Table 1. Cu:In Atomic Ratio of $CuInS_2$ Particles, Obtained by ICP-AES, for Two Different Copper Salts and for Different Temperatures of Addition (synthesis using method 1)

copper salt	temperature of the medium during the addition of the Li_2S suspension (°C)	Cu	In
CuI	25	7.52(1)	1
	5	2.94(6)	1
	−10	2.8(1)	1
CuCl	25	2.0(1)	1
	5	2.0(1)	1

Results and discussion

X-ray Diffraction and ICP-AES, Method 1. Figure 1 shows the X-ray diffractogram of the particles obtained from method 1. Two phases were identified, the $CuInS_2$ chalcopyrite (CH) structure (red line) and the Cu_2S chalcocite structure (blue line). Cu:In atomic ratios in the powder were determined by ICP-AES. When the reaction is done with a solution of one equivalent of copper and one equivalent of indium, a Cu:In ratio of 10:1 is obtained. The copper excess is represented by the Cu_2S phase. A double excess of indium was then used in order to decrease the amount of copper in the powder. The measured Cu:In ratio decreased to 7.52(1):1 when using CuI and such a double excess of indium at room temperature. Indium clearly does not react as fast as copper with sulfur. To decrease the reaction rate of copper with sulfur, the temperature of the reaction was lowered. At 5 °C, a Cu:In ratio of 2.94(6):1 was obtained, which became 2.8(1):1 at −10 °C (see Table 1). Lowering the temperature improves the Cu:In ratio but it is not possible to perform the reaction at lower temperatures because the NMI solutions become too viscous below −10 °C. However, when CuI was replaced by CuCl as the copper precursor salt, the Cu:In ratio came down to 2.0(1):1 at room temperature (Table 1). In this case, the temperature did not have any effect on the Cu:In ratio.

Suggested Mechanism, Method 1. Method 1 yields a mixture of $CuInS_2$ and Cu_2S; moreover, if the sulfur suspension is not added rapidly after the mixing of the copper and indium solutions, a CuS phase begins to appear (see the Supporting Information, S2 and S3, for details). As shown by XRD and ICP-AES analyses, the main problem arises from the very different reactivity of the metal cations with sulfur anions. It is not possible by either decreasing the temperature or by using a less reactive copper salt to obtain only $CuInS_2$ particles. According to the XRD and ICP-AES results, eq 1 is suggested

$$InCl_3 + CuI + 2Li_2S \rightarrow xCuInS_2 + (1-x)/2Cu_2S + (1-x)InCl_3 + 3xLiCl + LiI + 2 - (2x + (1-x)/2)Li_2S \quad 0 < x < 1 \qquad (1)$$

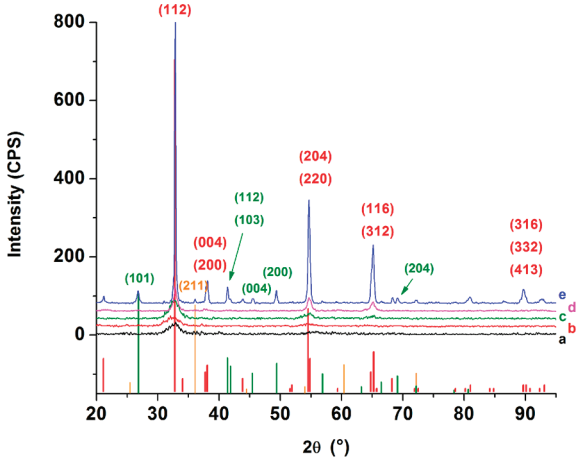

Figure 2. X-ray diffractograms of $CuInS_2$ particles obtained from experimental Method 2: (a) not annealed, and annealed for 2 h under a vacuum (100 mTorr) at (b) 200, (c) 300, (d) 400, and (e) 500 °C. In red lines at the bottom, the diffraction plans of the CH structure (JCPDS-ICDD card 27−0159[16]) and in green lines, the diffraction plans of the $LiInO_2$ phase (JCPDS-ICDD card 01−089−3853[42]).

This problem has been solved by mixing the $InCl_3$ solution and the Li_2S suspension first. This resulted in a transparent yellow solution, suggesting the formation of an indium−sulfur precursor. Then, when the copper source was added to this precursor solution, this yielded $CuInS_2$ particles with the appropriate stoichiometry for an n-type semiconductor.

X-ray Diffraction and Solid-State Raman Spectroscopy, Method 2. Figure 2 shows the diffractograms of $CuInS_2$ particles not annealed and annealed for 2 h at different temperatures under a vacuum. As expected, by increasing the annealing temperature, the diffraction peaks become sharper, which allows for better phase identification. The main diffraction peaks are assigned to the $CuInS_2$ chalcopyrite (CH) phase. Indeed, the peak positions correspond well to the JCPDS-ICDD card 27−0159;[16] this phase is shown as red lines in Figure 2. The highest annealing temperature used was 500 °C. Even under a vacuum, at this temperature, a slight oxidation shown by the presence of a $LiInO_2$ phase (see Figure 2e, green lines) is occurring. The cell parameters a and c were estimated from the observed 2θ angles of the diffraction peaks (112), (204)/(220), and (116)/(312) using Bragg's law and the CelRef3 software.[17] At 500 °C, the a and c parameters are 5.523(4) and 11.141(2) Å, respectively. These values are in agreement with the JCPDS-ICDD card 27−0159 for the $CuInS_2$ CH phase.[16] The full width at half-maximum (fwhm) of the (112) diffraction peak is used to estimate the crystallite size. Table 2 shows the crystallite size calculated for all the temperatures. At 200 and 300 °C, crystallites between 1.9 and 2.5 nm are obtained, which are smaller than the value of 4 nm obtained at 250 °C with a precursor of $(PPh_3)_2CuIn(SEt)_4$.[5] At 400 °C, a larger crystallite size of 6 nm is obtained, but this value is much

Table 2. Size of the $CuInS_2$ Crystallites Obtained after Annealing for 2 h at Different Temperatures under a Vacuum (100 mTorr), Estimated from XRD Data (synthesis using, Method 2)

temperature of annealing (°C)	crystallite size (nm)
not annealed	2.2
200	1.9
300	2.5
400	6.2
500	21.9

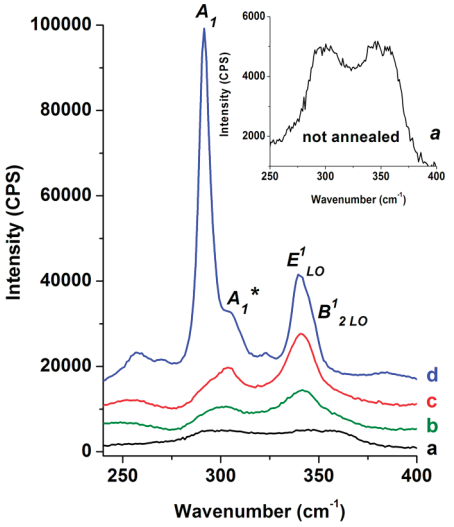

Figure 3. Raman spectra of $CuInS_2$ particles: (a) not annealed, and annealed for 2 h under a vacuum (100 mTorr) at (b) 300, (c) 400, and (d) 500 °C.

smaller than the one obtained by electrochemical growth, which led to a crystallite size of about 40 nm.[18,19] The particles annealed at 500 °C exhibit narrow diffraction peaks, which indicates a higher crystallinity. The fwhm of the main peak (112) is 0.3°, which leads to a crystallite size of about 22 nm.

As observed in our previous work,[8] it is possible that part of the $CuInS_2$ material crystallized in a CuAu structure,[20−22] but the latter has not been detected by XRD. Hence, Raman spectroscopy was also used to identify the crystalline phases. Figure 3 shows four main vibrational modes identified as follows: peaks A_1, E^1_{LO} and B^1_{2LO} are assigned to the CH crystalline phase,[22] whereas peak A_1* is assigned to the CuAu phase, as already demonstrated by Riedle[22] and Alvarez-Garcia[21] Peak A_1 is the main vibrational peak of the CH phase and peak A_1* is the main vibrational peak of the CuAu phase.

(16) Hahn, H., *Powder Diffraction File of Inorganic Phases #27−0159*; International Center for Diffraction Data: Newtown Square, PA, 1953.
(17) Bochu, B.; Laugier, J. *CelRef version 3*; Laboratoire des Matériaux et du Génie Physique de l'École Nationale Supérieure de Physique de Grenoble: Grenoble, France, 1987.
(18) Payment, F. Électrodéposition du semi-conducteur ternaire $CuInS_2$ pour utilisation dans une cellule photovoltaïque électrochimique. M.Sc. Thesis, Université du Québec à Montréal, Montreal, Canada, 2003.
(19) Morin, S. Déposition galvanostatique du semi-conducteur $CuInS_2$ sur un substrat de titane. M.Sc. Thesis, Université du Québec à Montréal, Montreal, Canada, 2006.
(20) Wei, S. H.; Zhang, S. B.; Zunger, A. *Phys. Rev. B* **1999**, *59*(4), R2478–R2481.
(21) Alvarez-Garcia, J. Characterisation of $CuInS_2$ films for solar cell applications by Raman Spectroscopy. Ph.D. Thesis, University of Barcelona, Barcelona, Spain, 2002.
(22) Riedle, T. Raman Spectroscopy for the Analysis of the Thin $CuInS_2$ Films. Ph.D. Thesis, Technical University of Berlin, Berlin, Germany, 2002.

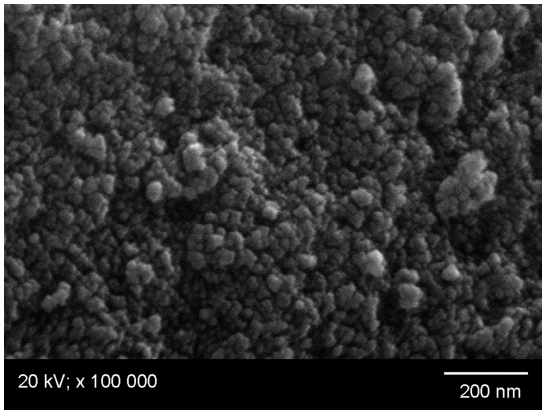

Figure 4. SEM image of a film of $CuInS_2$, deposited onto an ITO glass substrate and annealed under a vacuum for 2 h at 500 °C.

As shown in Figure 3 (and Figure 2), as the annealing temperature increases, the particles become more crystalline. It is then possible to identify both A_1 and A_1* peaks; their positions are 292−293 and 304−305 cm^{-1}, respectively. These values are in agreement with the literature.[8,21,22] Using a deconvolution technique with Gaussian peaks, A_1/A_1* ratios of 0.4 at 300 °C, 0.3 at 400 °C and up to 7 at 500 °C are obtained, indicating that the CH phase dominates following annealing at high temperature. At 500 °C, the thermal energy was sufficient to convert most of the metastable CuAu phase into the CH phase.[23] This should improve the device photoconversion efficiency since the CuAu phase is known to decrease the photovoltaic effect.[22] Moreover, the ratio of the positions of these two peaks, $\bar{\nu}(A_1/A_1$*), is 0.96−0.97, which is in agreement with Kondo et al.[24] and with our previous work.[8] Furthermore, no Raman peak at 475 cm^{-1}, indicative of Cu_xS phases,[21] was observed. The CuAu phase content is much lower than that observed in our previous work (A_1/A_1* ratio of 2)[8] and is closer to what is usually obtained via a gas phase synthetic method.[21]

Scanning Electron Microscopy, Method 2. Figure 4 shows a SEM image of the powder annealed at 500 °C. It shows relatively homogeneous particle sizes ranging from 50 to 100 nm. This is smaller than the size of particles obtained using triphenyl phosphite as a complexing agent and hexamethyldisilathiane as a sulfur source (200−500 nm),[8] which is quite large for our application. As previously mentioned, the Scherrer equation was used to determine the crystallite size from the XRD measurements; a value of about 22 nm was obtained. The particle size estimated using the SEM image provided a range of particle sizes larger than 22 nm. This is explained by the fact that SEM does not show the ultimate particles, but rather aggregates of smaller particles.

ICP-AES and EDX, Method 2. EDX and ICP-AES measurements were performed on $CuInS_2$ particles annealed at 500 °C; the results are shown in Table 3. EDX analysis gives a Cu:In:S ratio of 1:1.07(6):1.9(3) and ICP-AES measurements give a Cu:In ratio of 1:1.08(2). Both techniques show that the synthesized $CuInS_2$ particles have a bulk excess of indium of 7−8%, which should lead to n-type semiconductivity.

Table 3. Stoichiometry of $CuInS_2$ Particles Annealed at 500 °C, Obtained by EDX, ICP-AES, and XPS (Synthesis Using Method 2)

	Cu	In	S
EDX	1	1.07(6)	1.9(3)
ICP-AES	1	1.08(2)	
XPS 500 °C	1	1.19(1)	1.7(1)

X-ray Photoelectron Spectroscopy, Method 2. The surface of the $CuInS_2$ particles obtained after a thermal treatment at 500 °C was characterized by XPS. An XPS survey spectrum is shown in the Supporting Information, S4. Typical XPS spectra of the most intense peaks of the three main elements (Cu $2p_{3/2}$, In $3d_{5/2}$ and S 2p) are shown in Figure 5. Figure 5a shows a single copper $2p_{3/2}$ peak at a binding energy (B.E.) of 932.3(1) eV. The copper Auger parameter was calculated from the sum of the B.E. of the $2p_{3/2}$ XPS peak and the kinetic energy (K.E.) of the $L_3M_{45}M_{45}$ Auger peak (at 917.0(3) eV); it has a value of 1849.3 eV. Moreover, no shakeup peak at about 936 eV has been detected, which means that no copper oxidation occurred. The copper oxidation state is therefore +I.[25] The indium $3d_{5/2}$ XPS peak, at a B.E. of 444.5(1) eV (see Figure 5b), and the indium $M_4N_{45}N_{45}$ Auger peak, at a K.E. of 407.4(3) eV, give an Auger parameter of 851.9 eV, which suggests that the oxidation state of indium at the surface of the $CuInS_2$ particles is +III.[25] However, the B.E.s of the In $3d_{5/2}$ peak, when indium is bonded to sulfur or to oxygen, are very close. In our case, it is not possible to differentiate the indium of $CuInS_2$ from the indium of $LiInO_2$. The sulfur $2p_{3/2}$ XPS peak (see Figure 5c, right fitted peak) has a B.E. of 161.3(1) eV, which is typical of a sulphide (i.e., a sulfur bonded to copper or indium).[25] The absence of peaks between 168 and 170 eV confirms that there was no sulfur oxidation. The oxidation state of sulfur at the surface of the $CuInS_2$ particles is therefore-II.

Table 4 summarizes the positions of XPS and Auger peaks for copper, indium and sulfur. XPS peaks previously reported[8,26,27] have approximately the same B.E.s as those measured on samples produced in this work. Some small differences occur, mainly because of the use of adventitious carbon as a reference; the energy position used for the calibration was C 1s at 284.7 eV. To correct this, we used the Auger parameters and the following two other parameters: (i) Cu $2p_{3/2}$−S $2p_{3/2}$ and (ii) Cu $2p_{3/2}$−In $3d_{5/2}$. The values of these parameters are similar to those reported in the literature.[25−27] The main chemical elements

(23) Barcones, B.; Perez-Rodriguez, A.; Calvo-Barrio, L.; Romano-Rodriguez, A.; Morante, J. R.; Rudigier, E.; Luck, I.; Djordjevic, J.; Scheer, R. *Thin Solid Films* **2005**, *480*, 362–366.
(24) Kondo, K.; Nakamura, S.; Sato, K. *Jpn. J. Appl. Phys., Part 1* **1998**, *37*(10), 5728–5729.
(25) Moulder, J. F.; Stickle, W. F.; Sobol, P. E.; Bomben, K. D., *Handbook of X-ray Photoelectron Spectroscopy, A Reference Book of Standard Spectra for Identification and Interpretation of XPS Data*; Chastain, J., Ed.; Perkin-Elmer: Eden Prairie, MN, 1992.
(26) John, T. T.; Wilson, K. C.; Ratheesh Kumar, P. M.; Sudha Kartha, C.; Vijayakumar, K. P.; Kashiwaba, Y.; Abe, T.; Yasuhiro, Y. *Phys. Status Solidi A* **2005**, *202*(1), 79–84.
(27) Scheer, R.; Lewerenz, H. J. *J. Vac. Sci. Technol., A* **1994**, *12*(1), 56–60.

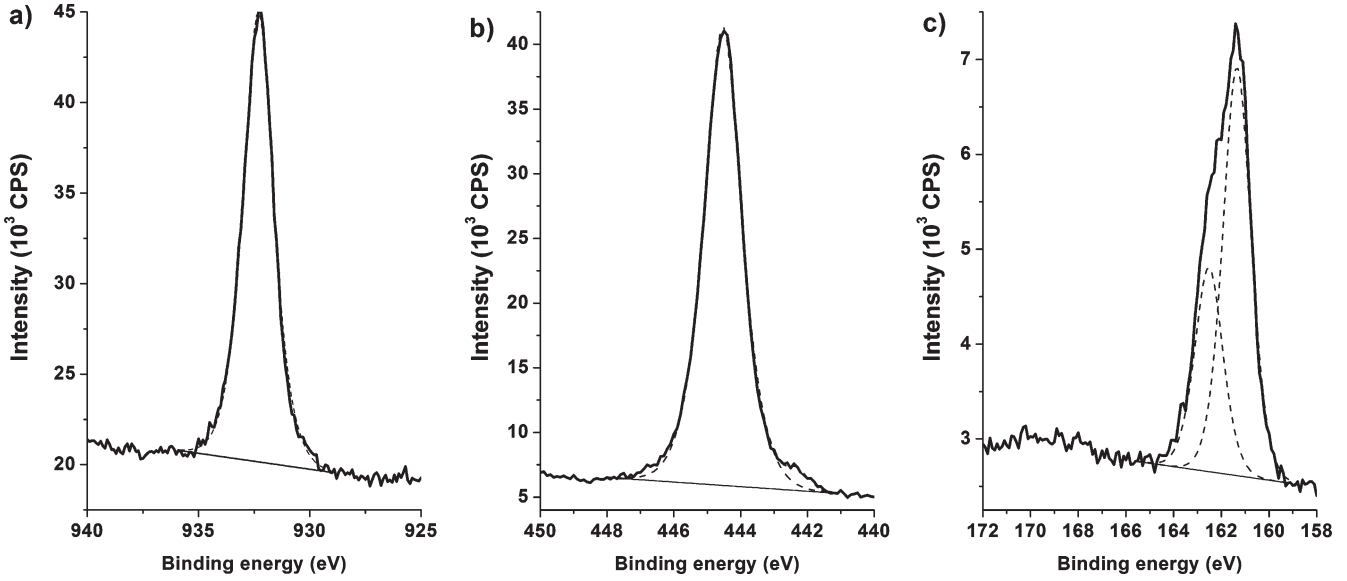

Figure 5. XPS: (a) Cu $2p_{3/2}$, (b) In $3d_{5/2}$, and (c) S $2p_{3/2}$ (right fitted peak) and $2p_{1/2}$ (left fitted peak) core level spectra of $CuInS_2$ particles annealed at 500 °C for 2 h under a vacuum (100 mTorr).

Table 4. XPS (B.E., binding energy) and Auger (K.E., kinetic energy) Peak Positions Obtained for $CuInS_2$ Particles Annealed for 2 h at 500 °C under Vacuum (see text for detail)

XPS and Auger peaks or Auger parameter	this work (eV)	previous method[8] (eV)	literature[26,27] (eV)
Cu $2p_{3/2}$	932.3(1)	932.7(1)	932.2−932.8
Cu $L_3M_{45}M_{45}$	917.0(3)	916.5(3)	
Cu Auger parameter	1849.3	1849.2	1848.9−1849.1
In $3d_{5/2}$	444.5(1)	445.0(1)	444.7−445.4
In $M_4N_{45}N_{45}$	407.4(3)	407.0(3)	
In Auger parameter	851.9	852.0	852.4−852.6
S $2p_{3/2}$	161.3(1)	161.8(1)	161.4−162.7
Cu$2p_{3/2}$−S $2p_{3/2}$	771.0	770.9(2)	770.0−770.2
Cu$2p_{3/2}$−In $3d_{5/2}$	487.8	487.7(2)	487.3−487.5

detected at the surface of the $CuInS_2$ particles are copper, indium and sulfur, along with some oxygen and carbon coming from the atmospheric contamination. Neither nitrogen nor chlorine, coming from the reagents and NMI, was detected. The surface composition of the particles, estimated from the XPS data, is $CuIn_{1.19(1)}S_{1.7(1)}$ (see Table 3). Therefore, the excess of indium is more significant at the surface than in the bulk of the material. This behavior has also been observed in our previous work but with an In excess of 45% at the surface.[8] Here, the difference between the surface and the bulk compositions is much smaller, resulting from a better control of the stoichiometry.

Herein, no chemical treatment (using KCN)[28] or electrochemical treatment (oxidation and dissolution of copper)[29,30] are needed to get n-type semiconductivity because the synthesis produces indium-rich $CuInS_2$ particles. Using a colloidal method with hexanethiol as a ligand, n-type $CuInS_2$ particles with an indium excess of 8% were obtained by Castro et al.[5] In this work, as

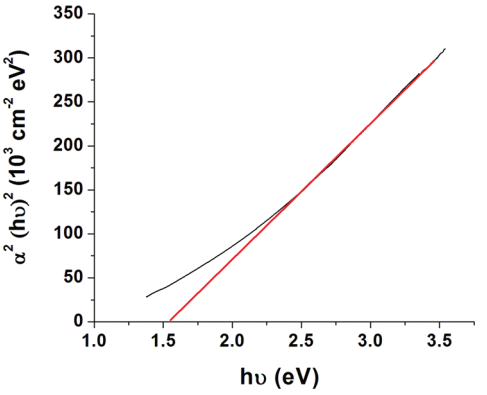

Figure 6. Plot of $(\alpha h\nu)^2$ versus photon energy ($h\nu$) for a 10 μm thick $CuInS_2$ film deposited onto an ITO conducting glass substrate. The particles were previously annealed at 500 °C for 2 h under a vacuum (100 mTorr).

discussed previously, a similar excess of about 7−8% was obtained in the bulk. This is lower than the value reported recently using another colloidal method,[8] indicating again a better control of the stoichiometry.

UV−Visible Spectroscopy, Method 2. The bandgap energy (E_g) of $CuInS_2$ particles annealed at 500 °C was determined by UV−visible spectroscopy. Ten micrometer thick $CuInS_2$ films prepared on ITO conducting glass substrates were used. Figure 6 shows the $(\alpha h\upsilon)^2$ vs $h\nu$ curve, where α is the absorption coefficient and $h\upsilon$ is the incident photon energy. The linear part of the curve indicates that $CuInS_2$ has a direct bandgap energy whose value is estimated at 1.55 eV from the intercept. This value is in good agreement with that of 1.5 eV reported in the literature.[4,31,32] In our previous work using another synthetic method,[7] a bandgap energy of 1.45 eV was obtained.

(28) Scheer, R. *Trends Vac. Sci. Technol.* **1997**, *2*, 77–112.
(29) Wilhelm, T.; Berenguier, B.; Aggour, M.; Kanis, M.; Lewerenz, H. J. *C. R. Chim.* **2006**, *9*(2), 294–300.
(30) Berenguier, B.; Lewerenz, H. J. *Electrochem. Commun.* **2006**, *8*(1), 165–169.
(31) Bihri, H.; Abd-Lefdil, M. *Thin Solid Films* **1999**, *354*(1−2), 5–8.
(32) Arici, E.; Sariciftci, N. S.; Meissner, D. *Adv. Funct. Mater.* **2003**, *13*(2), 165–171.

Table 5. Values of the Redox Potential (E_{redox}) and Fermi Level ($E_{F,el}$) of the T^-/T_2 and G^-/G_2 Redox Couples, and Majority Charge Carrier Densities (n_d), Flatband Potentials (V_{FB}) and Fermi Levels ($E_{F,sc}$) of $CuInS_2$ films Made of Particles Annealed at 500 °C under a Vacuum

redox couple	E_{redox} (V vs NHE)	$E_{F,el}$ (eV)	frequency (Hz)	n_d (cm^{-3})	V_{FB} (V vs NHE)	$E_{F,sc}$ (eV)
T^-/T_2	0.01	−4.51	5412	2.81×10^{18}	−0.87	−3.63
G^-/G_2	0.03	−4.53	3687	9.59×10^{18}	−1.40	−3.10

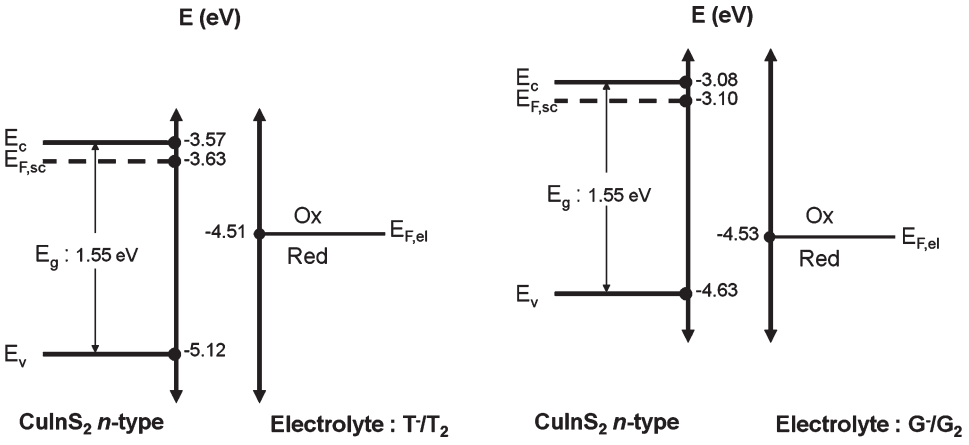

Figure 7. Energy level diagrams of a film of $CuInS_2$ immersed in two different redox couple solutions: T^-/T_2: 0.10 M HT, 0.01 M T_2, and 0.30 M TBAP in acetonitrile; and G^-/G_2: 0.0375 M KG, 0.0125 M G_2, and 0.30 M TBAP in EC-DMC.

The difference could be explained by the smaller particle sizes obtained in the present work.

Electrochemical Impedance Spectroscopy, Method 2. EIS measurements were carried out on $CuInS_2$ films made from particles annealed for 2 h at 500 °C. EIS analyses indicate the type of semiconductivity of $CuInS_2$, its majority charge carrier density (n_d) and Fermi level ($E_{F,sc}$, identified as the flatband potential, V_{FB}, in the dark). Measurements were done in the dark at room temperature using two different electrolyte solutions: (i) T^-/T_2 redox couple: 0.10 M HT, 0.01 M T_2, and 0.30 M TBAP (used as a supporting electrolyte) in acetonitrile; (ii) G^-/G_2 redox couple: 0.0375 M KG, 0.0125 M G_2, and 0.30 M TBAP in EC-DMC (50:50 (vol %/vol %)). Aqueous medium cannot be used in the type of cell we are developing because of the photocorrosion and photopassivation of low bandgap semiconductors that occur in water, as demonstrated by Gerischer and Goberecht.[33] This is the reason why organic redox couples soluble in organic solvents have been developed.[12−14]

A procedure described elsewhere was used to determine the semiconductor characteristics.[8] In this procedure, the $CuInS_2$ space-charge capacitance (C_{sc}) is calculated at various potentials from the Nyquist diagrams ($-Z_{im}$ vs Z_{real}, where Z_{im} and Z_{real} represent the imaginary and real component of the impedance, respectively). For both electrolytes, $|Z_{im}|$ measured at the highest frequency of the capacitive region were used to calculate C_{sc}: 5412 Hz for T^-/T_2 and 3687 Hz for G^-/G_2. This was done in order to minimize the detrimental effect of surface states that are more prominent at low frequency.[8] The positive slope of the Mott−Schottky plot ($1/C_{sc}^2$ vs applied potential) indicates that $CuInS_2$ is an n-type semiconductor, in agreement with the EDX, ICP-AES, and XPS analyses (excess of indium).

Table 5 gives the values of the redox potential (E_{redox}) and Fermi level ($E_{F,el}$) of the T^-/T_2 and G^-/G_2 redox couples, and majority charge carrier density (n_d), flatband potential (V_{FB},) and Fermi level ($E_{F,sc}$) of $CuInS_2$ films made of particles annealed at 500 °C. V_{FB} was calculated from the intercept of the linear part of the Mott−Schottky curve at $1/C_{sc}^2 = 0$, whereas n_d was determined from the slope. When the film was immersed in a solution containing the T^-/T_2 redox couple, the particles exhibited a V_{FB} of −0.87 V vs NHE, which corresponds to a semiconductor Fermi level of −3.63 eV. With the G^-/G_2 redox couple, a V_{FB} of −1.40 V vs NHE was obtained, which corresponds to a $E_{F,sc}$ of −3.10 eV. The majority charge carrier densities were calculated to be about 2.8×10^{18} cm^{-3} and 9.6×10^{18} cm^{-3} with T^-/T_2 and G^-/G_2, respectively. The energy level diagrams of the $CuInS_2$/electrolyte junctions are depicted in Figure 7. The T^-/T_2 and G^-/G_2 redox potentials of 0.01 and 0.03 V vs NHE, respectively, were measured using a platinum working electrode. On the vacuum scale, their Fermi levels ($E_{F,el}$) are −4.51 eV and −4.53 eV, respectively. As shown in Figure 7, $E_{F,el}$ lies between E_c and E_v, which is needed for the oxidation of T^- or G^- by the photogenerated holes to occur under illumination. The nature of the redox couple affects the $E_v - E_{F,el}$ value which is 0.61 eV with T^-/T_2 and 0.10 eV with G^-/G_2. This implies that there is a much better overlap of the G^- filled energy states (reduced species) with the $CuInS_2$ valence band, which would lead to a more efficient electron transfer under illumination (higher photocurrent). In our previous work using $CuInS_2$ particles synthesized via another colloidal method,[8] it was demonstrated that the G^- filled energy states also provide a good overlap with the $CuInS_2$

(33) Gerischer, H.; Goberecht, J. *Ber. Bunsen-Ges.* **1978**, *85*(5), 520–522.

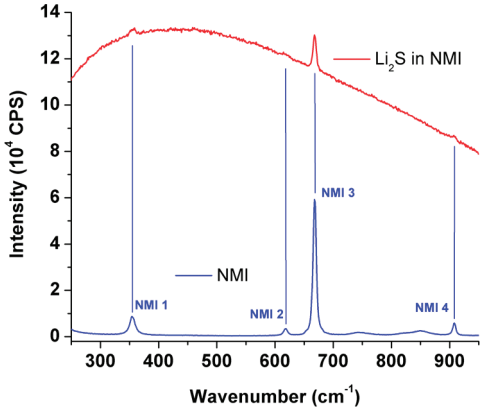

Figure 8. Raman vibrational spectra of NMI and of the Li_2S suspension in NMI (0.11 M).

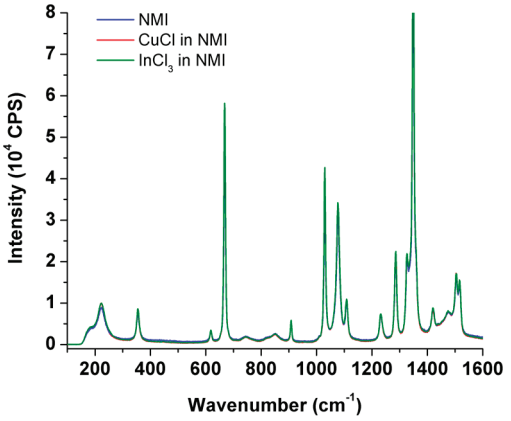

Figure 9. Raman vibrational spectra of NMI, of a solution of CuCl in NMI (0.060 M) and of a solution of $InCl_3$ in NMI (0.025 M).

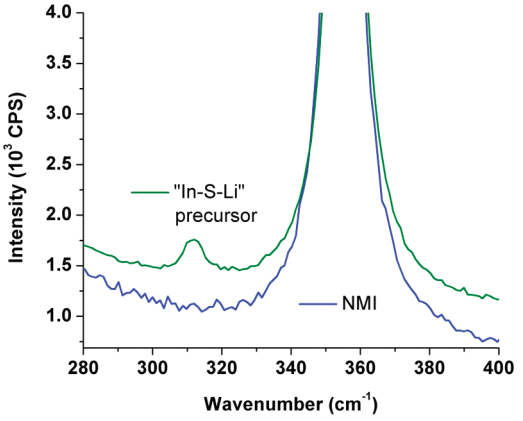

Figure 10. Raman vibrational spectra of NMI and of the indium−sulfur precursor solution recorded between 280 and 400 cm^{-1}.

valence band, with $E_v - E_{F,el} = 0.49$ eV. However, with the particles obtained using the current synthetic method, the overlap is even better.

The nature of the redox couple also affects $E_{F,sc}$, which ranges from −3.63 eV (T^-/T_2) to −3.10 eV (G^-/G_2), as indicated previously. The theoretical open-circuit photovoltage (V_{oc}) delivered by an electrochemical photovoltaic cell containing an n-type semiconductor is given by $E_{F,sc} - E_{F,el}$. Hence, the estimated V_{oc} values are 0.88 V (T^-/T_2) and 1.43 V (G^-/G_2). These interesting V_{oc} values are higher than those estimated when using $CuInS_2$ particles synthesized via an alternative colloidal method,[8] which are 0.56 and 0.89 V, respectively, with the T^-/T_2 and G^-/G_2 redox couples. Therefore, the G^-/G_2 redox couple should provide a device with greater photocurrent and photovoltage.

In situ Raman Spectroscopy, Method 2. It has been demonstrated that, in order to prevent the formation of a copper-rich phase, it is necessary to have a reaction between the indium and the sulfur salts, prior to the addition of the copper solution, to form an indium−sulfur precursor. The color change associated with the reaction between indium and sulfur suggests that a different reaction mechanism occurred compared to our previous work.[8] However, the present synthetic method still showed a predominance of indium at the surface of the particles but at a lower level. In-situ Raman spectroscopy measurements were therefore carried out to investigate the reaction mechanism of the formation of the particles. Figure 8 shows the Raman reference spectra of NMI and the Li_2S suspension in NMI. It is not possible to see any peak specific to Li_2S because of the large background induced by the light scattering of the suspension. Figure 9 shows the reference spectra of NMI, a solution of CuCl in NMI and a solution of $InCl_3$ in NMI. Absolutely no difference between the NMI and the metal solutions spectra is observed, which suggests that either no precursor was formed, and thus no metal-N bonds, or that such chemical bonds are not active in Raman spectroscopy. Therefore, unlike in our previous work,[8] it was not be possible to follow the disappearance of metal-N bonds during the addition of the copper solution. It has been previously observed that once the indium solution and the Li_2S suspension are mixed, a yellow transparent solution is obtained. Figure 10 shows the Raman spectrum of this precursor solution. The only difference between the NMI and precursor solution spectra is a peak observed at 311.7 cm^{-1}. Because the Li_2S Raman spectrum was too noisy, a simulation of the spectrum of the Li_2S molecule was done using Gaussian 98.[34] It showed two vibrational bands: 587 and 682 cm^{-1}.[35] Therefore, the peak at 311.7 cm^{-1} is likely not related to Li_2S but rather to the precursor. In addition, a Raman spectrum of In_2S_3 was measured and indeed In−S vibration bands range from 250 to 350 cm^{-1} (see the Supporting Information, S5). Thus, the peak at 311.7 cm^{-1} is assigned to the In−S bond.

(34) Frisch, M. J.; Trucks, G. W.; Schlegel, H. B.; Scuseria, G. E.; Robb, M. A.; Cheeseman, J. R.; Zakrzewski, V. G.; Montgomery Jr., J. A.; Stratmann, R. E.; Burant, J. C.; Dapprich, S.; Millam, J. M.; Daniels, A. D.; Kudin, K. N.; Strain, M. C.; Farkas, O.; Tomasi, J.; Barone, V.; Cossi, M.; Cammi, R.; Mennucci, B.; Pomelli, C.; Adamo, C.; Clifford, S.; Ochterski, J.; Petersson, G. A.; Ayala, P. Y.; Cui, Q.; Morokuma, K.; Malick, D. K.; Rabuk, A. D.; Raghavachari, K.; Foresman, J. B.; Cioslowski, J.; Octiz, J. V.; Stefanov, B. B.; Liu, G.; Liashenko, A.; Piskorz, P.; Komaromi, I.; Gomperts, R.; Martin, R. L.; Fox, D. J.; Keith, T.; Al-Laham, M. A.; Peng, C. Y.; Nanayakkara, A.; Gonzalez, C.; Challacombe, M.; Gill, P. M. W.; Johnson, B. G.; Chen, W.; Wong, M. W.; Andres, J. L.; Head-Gordon, M.; Replogle, E. S.; Pople, J. A. *Gaussian 98, revision A7*; Gaussian Inc.: Pittsburgh, PA, 1998.
(35) Courtel, F. M. Synthèses colloïdales de particules de $CuInS_2$ pour application en cellule photovoltaïque électrochimique. Ph.D. Thesis, Institut National de la Recherche Scientifique, Varennes-Montréal, Canada, 2007.

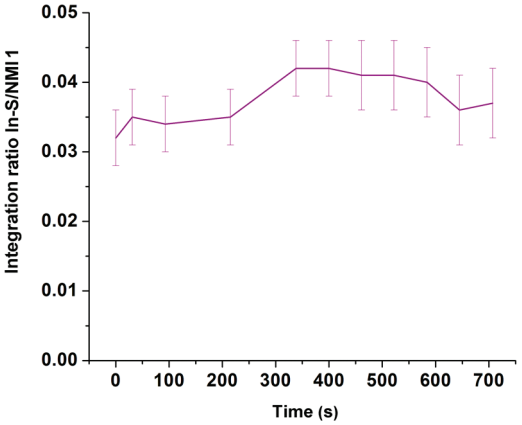

Figure 11. Graph of the integration ratio In−S/NMI1 as a function of time during the addition of the copper solution in the precursor solution at a rate of 0.08 mL min^{-1}.

A kinetic study has been carried out during the addition of the copper solution to the precursor solution. The variation of the In−S band was monitored during this addition. As more copper is added, the background intensity increases because of the light scattering induced by the $CuInS_2$ particles (see the Supporting Information, S6). Since NMI is the solvent, the intensity of its peak (NMI1) at about 350 cm^{-1} does not change with time; hence, it was used to normalize the variation of the integration of the In−S peak. As shown in Figure 11, the ratio of the integrated intensity of the Raman bands In−S/NMI1 does not vary significantly with time. It means that when copper reacts with this precursor to form $CuInS_2$, the In−S bond is not broken. It is possible that the formation of $CuInS_2$ occurs via a cationic exchange process: Li^+ ions from the precursor would be exchanged for Cu^+ ions. Such a process has been previously reported for the synthesis of $CuInS_2$ via a colloidal method,[36] and for the formation of $CuInO_2$ by a solid-state method via a $LiInO_2$ precursor.[37,38]

In this study, we did not perform any further characterization of the precursor molecule. A proposed reaction that might have occurred between $InCl_3$ and Li_2S, to form the precursor molecule, is shown by eq 2. Another likely reaction between the precursor and CuCl is shown by eq 3

$$InCl_3 + 2Li_2S \rightarrow [LiSInSLi]^+Cl^- + 2LiCl \quad (2)$$

$$[LiSInSLi]^+Cl^- + CuCl \rightarrow CuInS_2 + 2LiCl \quad (3)$$

In the method described in this work, the metal ions are not complexed with a strong ligand such as TPP[8] or oleylamine.[39,40] Thus, the copper reactivity with sulfur is unhindered. In these methods, the first step was the formation of a Cu(I)-S precursor, which led to the formation of Cu_2S nucleation sites phase prior to $CuInS_2$ formation. The second step corresponded to the indium insertion into the Cu(I)-S precursor to convert Cu_2S into $CuIn_xS_2$. Connor et al.[39] and Norako et al.[40] obtained p-type $CuInS_2$, whereas Courtel et al.[8] managed to obtain n-type $CuInS_2$. Furthermore, in the method described in this work, the inorganic negatively charged sulfur source (S^{2-}) also enhanced copper reactivity. As shown by the results from method 1, if indium and copper have to compete to react with sulfur, a Cu_2S phase is formed predominantly. Therefore, NMI does not balance copper and indium reactivity toward sulfur. This problem was resolved by the formation of an indium−sulfur precursor prior to the addition of the copper solution.

De Paz et al.[41] used the same concept and successfully synthesized $CuGaS_2$ by making a gallium-sulfur precursor (soluble in NMI) prior to the addition of the copper solution. We have tried to use In_2S_3 as an indium−sulfur precursor. In brief, In_2S_3 was suspended in NMI and a CuCl solution was added to the suspension. Unfortunately, no $CuInS_2$ phase was formed. Even though In_2S_3 was in a solid state, $Cu_{0.3}In_5S_{8.3}$ has been successfully synthesized via copper insertion into the In_2S_3 structure (see the Supporting Information, S7).

Conclusion

In this article, a new synthetic method for preparing $CuInS_2$ particles has been reported. This method uses NMI as a solvent and Li_2S as an inorganic sulfur source. XRD and Raman spectroscopy on powder showed a polycrystalline $CuInS_2$ material that crystallized in two different phases, the CH and the CuAu structures. Annealing the particles at higher temperature enhances the proportion of the CH phase which is preferred for photoelectrochemical devices. EDX, ICP-AES, and XPS analyses demonstrated that $CuInS_2$ particles with an excess of indium of about 7% in the bulk and 20% at the surface are obtained. Slight oxidation of the semiconductor was observed after annealing at 500 °C (XRD, weak $LiInO_2$ phase); however, no surface contaminants coming from the reactants are present, as was the case with the particles formed using a modified Czekelius's colloidal method.[8] UV−visible measurements indicate that the n-type $CuInS_2$ has a bandgap energy of 1.55 eV. Unlike most of the synthetic methods which produce p-type $CuInS_2$, this method produces particles with n-type semiconductivity. By using two different organic redox couples, EIS measurements confirmed the n-type semiconductivity. The $CuInS_2$ particles have Fermi levels of −3.63 eV

(36) Hu, H.; Yang, B.; Liu, X.; Zhang, R.; Qian, Y. *Inorg. Chem. Commun*. **2004**, *7*(4), 563–565.
(37) Shimode, M.; Sasaki, M.; Mukaida, K. *J. Solid State Chem*. **2000**, *151*(1), 16–20.
(38) Sasaki, M.; Shimode, M. *J. Phys. Chem. Solids* **2003**, *64*(9−10), 1675–1679.
(39) Connor, S. T.; Hsu, C.-M.; Weil, B. D.; Aloni, S.; Cui, Y. *J. Am. Chem. Soc*. **2009**, *131*(13), 4962–4966.
(40) Norako, M. E.; Franzman, M. A.; Brutchey, R. L. *Chem. Mater*. **2009**, *21*(18), 4299–4304.
(41) De Paz, H.; Cirtiu, M. C.; Marsan, B. Synthesis and Characterization of Semiconducting $CuGaS_2$ Nanoparticles for Water Photoelectrolysis.In *215th Meeting of the Electrochemical Society Abstracts*, San Francisco, May 24−29, 2009; The Electrochemical Society: Pennington, NJ, 2009; p 530.
(42) Hoppe, R.; Schepers, B., *Powder Diffraction File of Inorganic Phases #01−089−3853*; International Center for Diffraction Data: Newtown Square, PA, 1958.

and −3.10 eV, and majority charge carrier densities of 2.8×10^{18} and 9.6×10^{18} cm^{-3} with T^-/T_2 and G^-/G_2 redox couples, respectively. The G^-/G_2 redox couple shows a better overlap of the redox filled states with the semiconductor valence band (expected higher photocurrent) and a greater open-circuit photovoltage estimated at 1.43 V.

Results obtained from our previous work[8] and from the present work show that the complexation of the metal ions and the negative charge on sulfur anions (organic source like hexamethyldisilathiane versus inorganic source like Li_2S) play a key role in the mechanism of formation of $CuInS_2$ particles. Indeed, when no complexing agent, such as TPP, is used, copper reacts too quickly with sulfur (compared to indium), leading to a copper-rich powder. If an indium−sulfur precursor is formed before sulfur reacts with copper, a much better control of the n-type $CuInS_2$ properties is obtained. Both studies also provide chemical insights into the growth mechanism of n-type $CuInS_2$ particles which contain an excess of the metal that is less reactive. They also explain why, in most methods, p-type $CuInS_2$ particles (with an excess of copper) are obtained if no special care (i.e., precursor) is taken to control the reactivity of copper and indium. On the other hand, the use of a ligand, such as TPP, slows down the metal ion reactivity, more specifically Cu^+. Finally, the colloidal synthetic method presented in this work can be used to prepare other ternary or binary semiconducting compounds, such as CdS, $CuGaS_2$, etc.[9]

Acknowledgment. The authors acknowledge the financial support of the Natural Sciences and Engineering Research Council of Canada (NSERC), the Fonds québécois de la recherche sur la nature et les technologies (FQRNT), Valorisation-Recherche Québec (VRQ), Gestion Valéo s.e.c., the Institut National de la Recherche Scientifique (INRS), and the Université du Québec à Montréal (UQÀM).

Supporting Information Available: The structure of the two redox couples used for the electrochemical measurements; the UV−visible spectra of $InCl_3$, CuCl, $CuCl_2$, and $InCl_3 + CuCl$; the cyclic voltamogramms of $InCl_3$, CuCl, and CuI; the XPS survey spectrum of the $CuInS_2$ particles; the Raman spectrum of In_2S_3; the Raman spectra of the precursor solution during the addition of a solution of CuCl; and the synthesis, and XRD and SEM analyses of $CuIn_5S_8$ (PDF). This material is available free of charge via the Internet at http://pubs.acs.org.